

MuscleMap: Towards Video-based Activated Muscle Group Estimation in the Wild

Kunyu Peng, David Schneider, Alina Roitberg, Kailun Yang*, Jiaming Zhang, Chen Deng, Kaiyu Zhang, M. Saquib Sarfraz, and Rainer Stiefelhagen

Abstract—In this paper, we tackle the new task of video-based Activated Muscle Group Estimation (AMGE) aiming at identifying active muscle regions during physical activity in the wild. To this intent, we provide the MuscleMap dataset featuring >15K video clips with 135 different activities and 20 labeled muscle groups. This dataset opens the vistas to multiple video-based applications in sports and rehabilitation medicine under flexible environment constraints. The proposed MuscleMap dataset is constructed with YouTube videos, specifically targeting High-Intensity Interval Training (HIIT) physical exercise in the wild. To make the AMGE model applicable in real-life situations, it is crucial to ensure that the model can generalize well to numerous types of physical activities not present during training and involving new combinations of activated muscles. To achieve this, our benchmark also covers an evaluation setting where the model is exposed to activity types excluded from the training set. Our experiments reveal that the generalizability of existing architectures adapted for the AMGE task remains a challenge. Therefore, we also propose a new approach, TRANSM³E, which employs a multi-modality feature fusion mechanism between both the video transformer model and the skeleton-based graph convolution model with novel cross-modal knowledge distillation executed on multi-classification tokens. The proposed method surpasses all popular video classification models when dealing with both, previously seen and new types of physical activities. The contributed dataset and code are made publicly available at <https://github.com/KPeng9510/MuscleMap>.

Index Terms—Video-based activated human muscle group estimation, multi-modal learning, human motion attribute analysis.

I. INTRODUCTION

Human activity understanding is important as it enables the development of applications and systems that can enhance healthcare, improve security, and optimize various aspects

This work was supported in part by the SmartAge project sponsored by the Carl Zeiss Stiftung (P2019-01-003; 2021-2026), in part by the University of Excellence through the “KIT Future Fields” project, in part by the Helmholtz Association Initiative and Networking Fund on the HoreKA@KIT partition, and in part by Hangzhou SurImage Technology Company Ltd.

K. Peng, D. Schneider, J. Zhang, M. S. Sarfraz, and R. Stiefelhagen are with the Institute for Robotics and Anthropomatics, Karlsruhe Institute of Technology, Germany (email: firstname.lastname@kit.edu).

A. Roitberg is with the Institute for Artificial Intelligence, the University of Stuttgart, Germany (email: alina.roitberg@f05.uni-stuttgart.de).

K. Yang is with the School of Robotics and the National Engineering Research Center of Robot Visual Perception and Control Technology, Hunan University, China (email: kailun.yang@hnu.edu.cn).

C. Deng is with the School of Sports Science, Beijing Sport University, China (email: dengchen@bsu.edu.cn).

K. Zhang is with the School of Sports Engineering, Beijing Sport University, China (email: kaiyuzhang@bsu.edu.cn).

M. S. Sarfraz is also with Mercedes-Benz Tech Innovation, Germany.

*Corresponding author: Kailun Yang.

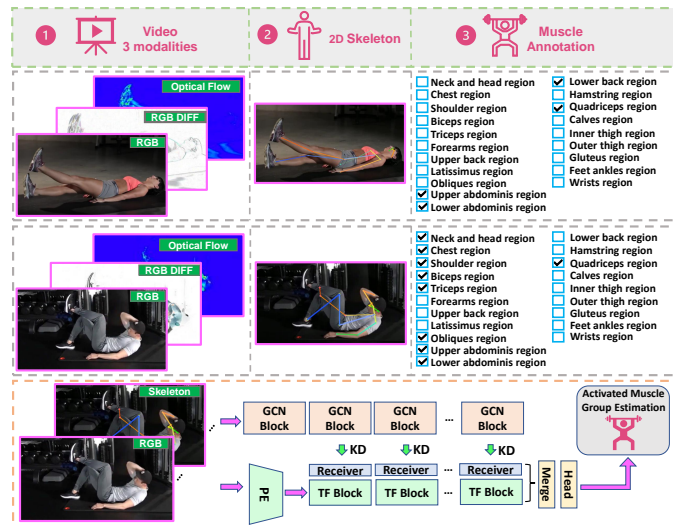


Fig. 1: Overview of the proposed MuscleMap dataset (Top) and the TRANSM³E model (Bottom). Our dataset contains four data modalities, *i.e.*, RGB, RGB difference (RGB Diff), optical flow, and 2D skeleton. PE and TF denote the patch embedding layer and the transformer block, respectively.

of daily life by automatically identifying and understanding human actions and behaviors [1], [2], [3], [4], [5], [6]. Knowing which skeletal muscles of the human body are activated benefits human activity understanding, and sport and rehabilitation medicine from multiple perspectives and prevents inappropriate muscle usage which may cause physical injuries [7]. In health care, patients need to know how to conduct the exercise correctly to recover from surgery [8] or specific diseases [9], *e.g.*, COVID-19 [10]. Knowledge about muscle activations allows for user-centric fitness applications providing insights for everyday users or professional athletes who need specially adapted training. The majority of existing work on Activated Muscle Group Estimation (AMGE) is based on wearable devices with electrode sensors [11]. Yet, many wearable devices are inconvenient and heavy [12], even harmful to health [13], and have limited usage time due to the battery [14]. A big strength of wearable devices is the high accuracy achieved through direct signal measurement from skin or muscle tissue. However, such exact bio-electrical changes are not required in a large number of medical recovery programs, and knowing the binary activation status of the muscle as shown in Figure 1 is sufficient in many situations [15],

[16], [17]. In contrast to wearable devices, most people have a video camera available at hand on their phone or laptop. Applying video-based AMGE on in-the-wild data collected by using smartphones or other widely available smart devices would allow for the application of such programs even without access to specialized hardware. Thereby, end-to-end video-based AMGE approaches are expected to be developed to prevent overburdens caused by wearable devices from both physical and psychological points of view. *Can modern deep learning algorithms relate fine-grained physical movements to individual muscles?* To answer this question, we tackle the barely researched task of video-based active muscle group estimation under an in-the-wild setting, which estimates muscle contraction during physical activities from video recordings without a restricted environment and background constraints.

Current research in video-based AMGE is limited by small-scale datasets and constrained data collection settings [18], where the data is often annotated with sensor signals and confined to restricted environments, covering only a limited range of actions. However, with the expansion of deep learning model capacities, there is a pressing need for larger datasets encompassing a wider variety of environments and activities. This expansion is vital for advancing the field of video-based AMGE within the research community.

In this work, we collect the first large-scale in-the-wild AMGE dataset from YouTube without environment constraints and give binary activation for different muscle regions by inquiring about sports field researchers. We created the MuscleMap dataset — a video-based dataset with 135 different exercises collected from YouTube considering in-the-wild videos. Each exercise type is annotated with one or multiple out of 20 different muscle group activations, as described in Table I, which opens the door for video-based activated muscle group estimation in the wild task to the community. We annotate the dataset in a multi-label manner since human body movement is produced by the coordinated operation of diverse muscle regions. To acquire such annotations, we first do statistical reasoning based on >400 online fitness- and healthcare resources and then ask biomedical and sports researchers to give a final correction on each annotation.

We select various off-the-shelf Convolutional Neural Networks (CNNs) [19], [20], Graph Convolutional Networks (GCNs) [21], [22], [23], and transformer-based architectures [24], [25], [26] from human activity recognition field together with statistic methods as baselines. Our proposed MuscleMap benchmark describes a multi-label classification problem where each sample might be annotated with one or up to twenty labels. However, we find that it is challenging for all these models when they deal with new activity types containing new activated muscle combinations at test time considering the AMGE generalizability. Skeleton-based models are observed to show good performance on the new activity types while working not well on known activity types. The video-based models show good performance on the known activity types while delivering limited performance on the new activity types. An approach that can work well on both known and new activity types is thereby expected.

To tackle the aforementioned issue, we propose

TABLE I: A comparison among the statistics of the video-based datasets, where AR, AQA, and CE indicate activity recognition, activity quality assessment, and calorie consumption estimation.

Dataset	NumClips	Task	MultiLabel	NumActions
KTH [28]	599	AR	False	6
UCF101 [29]	13,320	AR	False	101
HMDB51 [30]	6,849	AR	False	51
ActivityNet [31]	28,108	AR	False	200
Kinetics400 [31]	429,256	AR	False	400
Video2Burn [32]	9,789	CE	False	72
MTL-AQA [33]	1,412	AQA	True	/
FineDive [34]	3,000	AQA	True	29
FineGym [35]	32,697	AQA	True	530
MuscleMap136 (Ours)	15,004	AMGE	True	135

TRANSM³E, a cross-modality knowledge distillation and fusion architecture that combines RGB and skeleton data via a new classification tokens-based knowledge distillation and fusion mechanism. To achieve better extraction of underlying cues for AMGE, we propose and equip TRANSM³E with three essential novel components, *i.e.*, *Multi-Classification Tokens (MCT)*, *Multi-Classification Tokens Knowledge Distillation (MCTKD)*, and *Multi-Classification Tokens Fusion (MCTF)*, atop the most competitive performing architecture MVITv2 [25] as the backbone. As it is fundamental to mine and predict the activities at the global level for AMGE, the proposed TRANSM³E, appearing as a transformer-based approach, is endowed with the capacity for long-term reasoning of visual transformers [27]. Since AMGE is a multi-label classification task, MCT is introduced, in view that using more classification tokens is expected to introduce more benefits toward finding informative cues. MCT also builds up the base for cross-modality MCT-level knowledge distillation.

Knowledge distillation [36] is leveraged for cross-modality knowledge transfer after the feature map reduction of the transformer block to enable a more informative latent space learning for different modalities. Transferring cross-modality knowledge during training significantly benefits the model in finding out cross-modality informative cues for the AMGE task. However, we find that it is difficult to achieve the knowledge distillation between two models with obvious architecture differences, *e.g.*, graph convolutional networks (GCNs) and video transformers, considering the alignment of the feature maps coming from different backbones and modalities to achieve the appropriate and effective knowledge distillation. Aside from the architectural differences, we examine that using late fusion to fuse the skeleton-based model and video-based model can not achieve a satisfactory performance due to the lack of alignment of the two different feature domains.

We thereby propose a cross-modality MCT-level knowledge distillation scheme considering knowledge distillation on the intermediate and final layers by specifically designing a knowledge distillation MCT for the model of each modality. Alongside the MCT used solely for the classification, we leverage another MCT to execute the knowledge distillation for each modality. The cross-modality knowledge distillation is then executed only between the knowledge distillation MCTs from the two modalities, while the existing works mostly use

knowledge distillation calculated from the full embeddings or single knowledge distillation token at the final layer, and use a larger teacher [36], [37], [38], [39], [40].

While the mentioned MCTKD mechanism integrates cross-modal knowledge into our main network with additional MCT for the knowledge distillation, another contribution, MCTF, merges the MCT of the distilled knowledge and the MCT for classification to achieve a final prediction towards the active muscle regions during human body motion for each modality. By combining these three components, TRANSM³E achieves state-of-the-art performances with superior generalizability compared to the tested baselines.

In summary, our contributions are listed as follows:

- We open the vistas of video-based Activated Muscle Group Estimation in the wild task with the aim of lowering the threshold of entry to muscle-activation-based health care and sports applications.
- We provide a new benchmark MuscleMap to propel research on the aforementioned task which includes the large-scale *MuscleMap* dataset. We also present a large number of baseline experiments for this benchmark, including CNN-, transformer-, and GCN-based approaches.
- We especially take the evaluation of the generalizability into consideration by constructing test and validation sets using new activities excluded during the training.
- We propose TRANSM³E, targeting improving the AMGE generalizability towards new activity types. *Multi-classification Tokens* (MCT), *Multi-Classification Tokens Knowledge Distillation* (MCTKD) and *Multi-Classification Tokens Fusion* (MCTF) are used to formulate TRANSM³E, which shows superior generalizability on new activities and introduces state-of-the-art results on the MuscleMap benchmark.

II. RELATED WORK

Activate Muscle Group Estimation (AMGE) analysis is predominantly performed using electromyographic (EMG) data [41], [42] either with intramuscular (iEMG) or surface EMG sensors (sEMG). These methods use EMG data as input and detect activated muscle groups to achieve an understanding of the human body movement and the action, while we intend to infer muscle activations from body movements, therefore describing the opposite task. Chiquier *et al.* [18] propose a video-based AMGE dataset by using the signal of the wearable devices as the annotation. Yet, the data collection setting and the environment are restricted. The scale of the introduced dataset is relatively small and it encompasses limited action types. In our work, we collect a large-scale dataset based on HIIT exercises on YouTube while delivering binary annotation for each muscle region. We reformulate it into a multi-label classification task, namely AMGE in the wild. The annotations are first derived from online resources and then checked and corrected by researchers in biomedical and sports fields.

Activity Recognition is a dominating field within visual human motion analysis [1], [2], [3], [4], [5] which was propelled by the advent of Convolutional Neural Networks (CNNs) with 2D-CNNs [43] in combination with recurrent neural networks

(RNNs) [44] or different variations of 3D-CNNs [19], [20], [45]. More recently, transformer-based methods advanced over 3D-CNNs, especially with advanced pre-training methods and large datasets [25], [26], [46]. Action Quality Assessment (AQA) [33], [47] and Visual Calory Estimation (VCE) [32] relate to our work since these methods likewise shift the question of research from *what?* to *how?* with the aim of detailed analysis of human motion. Multimodal data is a common strategy, *e.g.*, by combining RGB video with audio [48], [49], [50], poses [51], optical flow [48], or temporal difference images [52]. Body poses are commonly used as a modality for activity recognition on their own. Yan *et al.* [21] and follow-up research [22], [23], [53], [54] make use of GCNs, while competitive approaches leverage CNNs with special pre-processing methods [55], [56].

Knowledge distillation (KD) [36] became a common technique to reduce the size of a neural network while maintaining performance. In review [57], methods can be categorized to focus on knowledge distillation based on final network outputs (response-based) [58], [59], based on intermediate features (feature-based) [60], [61], or based on knowledge about the relations of data samples or features (relation-based) [62]. Recently, adaptations of distillation for transformer architectures gained attraction [40], [63]. Fusion strategies can be grouped into feature-fusion [64] and score fusion [65].

Multi-label classification methods allow for assigning more than a single class to a data sample. Common strategies include per-class binary classifiers with adapted loss functions to counter the imbalance problem [66], methods that make use of spatial knowledge [67], [68], methods that make use of knowledge about label relations [69], [70], or methods based on word embeddings [71], [72].

Datasets which combine visual data of the human body with muscle activation information are sparse and mainly limited to specific sub-regions of the human body, *e.g.*, for hand gesture recognition [73]. In contrast, a large variety of full-body human activity recognition datasets were collected in recent years, which are labelled with high-level human activities [30], [74], fine grained human action segments [75], [76], or action quality annotations [35]. We leverage such datasets by extending them with muscle group activation labels.

III. BENCHMARK

In this section, we introduce the details of our proposed MuscleMap benchmark for video-based activated muscle group estimation in the wild task, including the contributed dataset, the annotation, the evaluation protocols, the evaluation metrics, and the baselines. Note, that the selected activities in the MuscleMap dataset are specifically chosen based on fitness and health-care-related resources under unconstrained background and environment settings.

A. MuscleMap Dataset

With the new video-based active muscle group estimation in-the-wild task in mind, we collect the MuscleMap dataset by querying YouTube for physical exercise video series. The collected dataset contains 135 activity types as well as 15,004

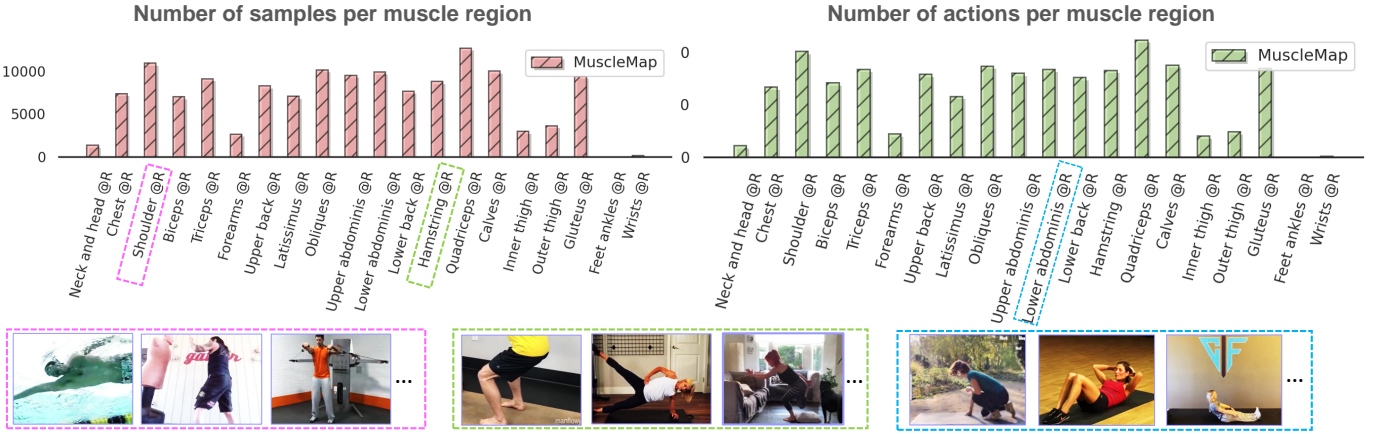


Fig. 2: An overview of the number of samples and the number of activity types per muscle region (@R), depicted at the top left and the top right. On the bottom, some activity-specific samples from the MuscleMap dataset are shown according to the corresponding muscle group.

video clips and is competitive compared to other video-based datasets targeting fine-grained tasks, as shown in Table I. Twenty activities are reserved for the validation and test splits of new activities, which are not included in the training set.

MuscleMap targets physical exercise videos from fitness enthusiasts. High-Intensity Interval Training (HIIT) exercises are well suited for the AMGE in-the-wild task since they display a large range of motions that are designed to activate specific muscle groups and instructional videos provide high-quality examples of the displayed motion. The collected videos in our dataset are mostly near-person, which can benefit video-based muscle contribution understanding for the in-the-wild videos. A small set of activities from the MuscleMap dataset is shown in the bottom part of Figure 2. In Table I, MuscleMap is compared with existing human activity recognition, action quality assessment, and calorie consumption datasets.

B. Activated Muscle Group Annotation

We cluster skeletal muscles of the human body into 20 major muscle groups with binary activation as shown in the checkboxes in Figure 1. We thereby provide binary annotations for these commonly leveraged human body muscles according to these 20 muscle region classes, *i.e.*, *neck and head region*, *chest region*, *shoulder region*, *biceps region*, *triceps region*, *forearms region*, *upper back region*, *latissimus region*, *obliques region*, *upper abdominis region*, *lower abdominis region*, *lower back region*, *hamstring region*, *quadriceps region*, *calves region*, *inner thigh region*, *outer thigh region*, *gluteus region*, *feet ankles region*, and *wrists region*. We rearrange *occipitofrontalis*, *temporoparietalis*, *levator labii superioris*, *masticatorii*, *sternocleidomastoideus* as *neck and head muscle region*; *pectoralis major* as *chest region*; *deltoides* as *shoulder region*; *biceps brachii* as *biceps region*; *triceps brachii* as *triceps region*; *flexor carpi radialis*, *palmaris longus*, *abductor pollicis longus* as *forearm region*; *trapezius* as *upper back region*; *latissimus dorsi* as *latissimus region*; *external oblique*, *serratus anterior* as *obliques region*; *rectus abdominis*, *quadratus lumborum* as *upper abdominis region*;

transversus abdominis, *pyramidalis* as *lower abdominis region*; *erector spinae* as *lower back region*; *biceps femoris*, *semimembranosus*, *semitendinosus* as *hamstring region*; *rectus femoris*, *vastus medialis* as *quadriceps region*; *gastrocnemius*, *soleus* as *calves region*; *adductor longus*, *sartorius*, *gracilis* as *inner thigh region*; *iliotibial tract* as *outer thigh region*; *gluteus maximus* as *gluteus region*; *peroneus longus and brevis*, *extensor digitorum longus*, *flexor hallucis longus*, *flexor digitorum longus*, *peroneus tertius*, *tibialis posterior* as *feet ankles region*; *extensor pollicis*, *1st dorsal interosseous*, *pronator quadratus* as *wrists region*.

As sources from sports experts have been successfully used as annotation sources in similar problems [33], the pairing of muscle group activations to physical activities is preliminarily derived from >400 health care and fitness resources reported by well-established fitness and sports coaches and comprehensive scientific research works of physical activity, *e.g.*, [77], [78]. These resources label a set of primary activated muscles. After constructing a mapping of physical activities and the activated muscle groups using the aforementioned sources, we employ a label noise suppression mechanism to ensure high-quality annotations.

First, to maintain the AMGE diversity, we take the activity granularity and variants into consideration. Note, that different variants always have different annotations. To avoid noisy labels, we use statistical majority voting following the ImageNet1K [79] protocol to achieve preliminary label denoising. This protocol ensures agreement among different sources: a muscle group label is considered reliable for a certain physical activity only if multiple scientific- and expert sources agree on its activation and there are no considerable inconsistencies among the sources. To further ensure the quality of the annotation, we ask 2 researchers from the biomedical and sports fields to further check our annotations and make corrections. If the two biomedical researchers fully agree with one correction proposal then the annotation correction is executed after an in-depth discussion.

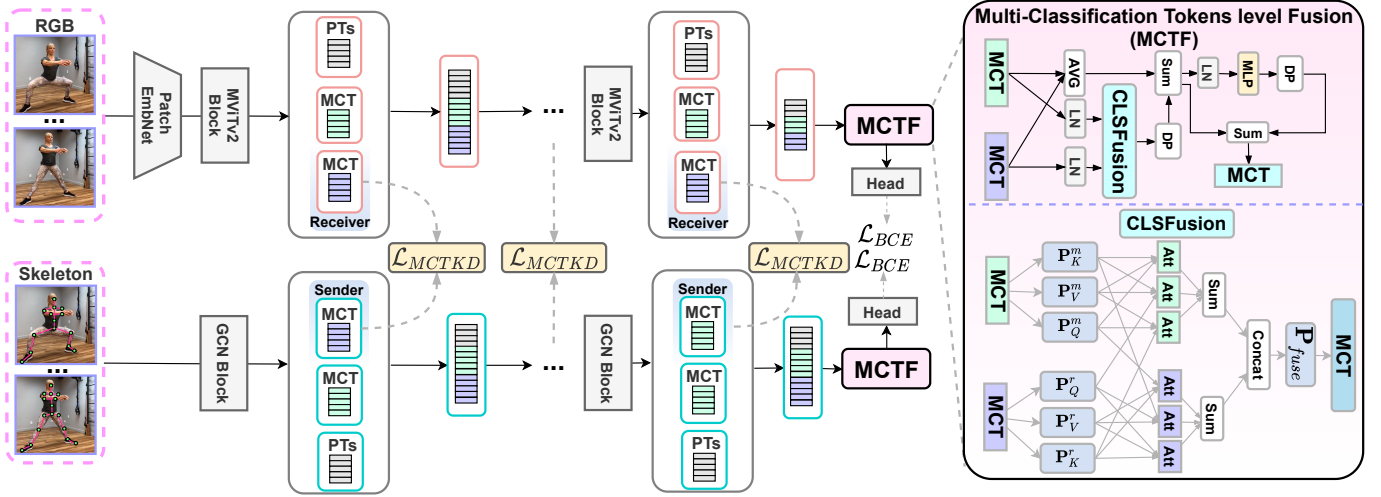


Fig. 3: **TRANSM³E**. The knowledge is distilled from the RGB Difference (Diff) to the RGB, PTs denote the patch embedding tokens. Three main components are shown, *e.g.*, Multi-Classification Tokens (MCTs), Multi-Classification Tokens Knowledge Distillation (MCTKD), and Multi-Classification Tokens Fusion (MCTF).

C. Evaluation Protocol

To evaluate the generalizability of the leveraged approaches for the AMGE in-the-wild task, we formulate the **new val/test** and **known val/test**, where we use val and test to indicate the validation set and the test set, respectively. For MuscleMap, 20 of 135 activities are leveraged to formulate the **new val/test** set, which are *hollow hold, v-ups, calf raise hold, modified scissors, scissors, reverse crunches, march twists, hops on the spot, up and down planks, diamond push ups, running, plank jacks, archer push ups, front kicks, triceps dip hold, side plank rotation, raised leg push ups, reverse plank kicks, circle push ups, and shoulder taps*. The activity types for the **known test** and **known val** are the same as the activity types in the training set. The sample number for train, **new val**, **known val**, **new test**, **known test** sets are 7,069, 2,355, 1,599, 2,360, and 1,594. The performances are finally averaged for new and known sets (**mean test** and **mean val**). We randomly pick up half of the samples from each **new** activity type to construct the **new val** while the rest of the samples from the selected **new** activities are leveraged to construct the **new test**. After the training of the leveraged model, we test the performance of the trained model on **known/new** evaluation and **known/new** test sets, and then average the performance of **known** and **new** sets to get the averaged performance on evaluation and test sets by considering both **known** and **new** activities which are both important for the AMGE in-the-wild task.

D. Evaluation Metric

Mean averaged precision (mAP) is used as the evaluation metric for the AMGE in-the-wild task. Assuming that $l_i, i \in 1, N_{new\ test}$ is the multi-hot annotation for the sample i in the **new test** set and $Preds_i, i \in 1, N_{new\ test}$ is the prediction of the model for the given sample i , we first concatenate the labels to get the label vector L . We first select the subset of the concatenated list of $Preds$ and L by calculating the mask through $m = (L == 1)$. The corresponding subsets are

thereby denoted as $Preds[m]$ and $L[m]$. Then we calculated the mean averaged precision score using the function and code from sklearn [80].

E. Baseline Methods

Video classification approaches, *e.g.*, I3D [19], SlowFats [20], and MVITv2 [25], skeleton approaches, *i.e.*, ST-GCN [21], CTR-GCN [22], and HD-GCN [23], and statistic calculations, *e.g.*, randomly guess (Random), are selected as baselines to formulate our MuscleMap benchmark on the proposed new dataset to achieve AMGE in-the-wild. Statistic calculation-based approaches serve for performance verification considering the question regarding whether the prediction of the model is random or not. Skeleton-based approaches are selected since they directly take the geometric relationship of the human body into consideration without disrupting information from the background. Considering video-based approaches, transformer-based models, *i.e.*, MVITv2 and VideoSwin, and Convolutional Neural Network (CNN) based models, *i.e.*, C2D, I3D, Slow, and SlowFast, are leveraged. Transformers are expected to have better performance compared with CNNs due to their excellent long-term reasoning ability [27], which is also verified in the experiments conducted on the MuscleMap benchmark.

IV. ARCHITECTURE

A. Preliminaries of MVIT

TRANSM³E is based on the improved multi-scale visual transformer (MVITv2) [25], which is based on MVITv1 [24]. The model architecture of TRANSM³E is shown in Figure 3. Compared with ViT [81], MVITv1 increases the channel resolution progressively and reduces the resolution on the spatiotemporal plane simultaneously, which realizes pooling operations both on Keys (K) and Queries (Q). The basic idea of MVITv1 is the construction of different low- and high-level visual modeling stages [24]. Multi-scale pooling attention

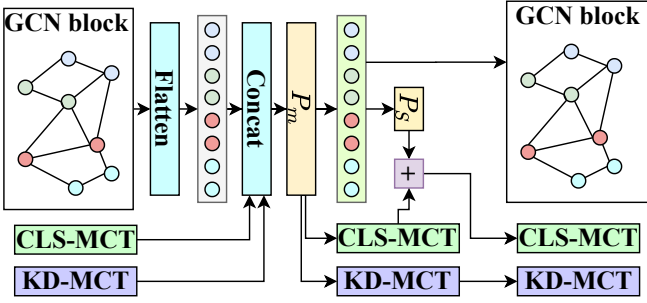


Fig. 4: An overview of the modified GCN block with knowledge distillation MCT and classification MCT.

is one of the major components of MVitv2 compared with ViT. MVitv2 uses decomposed relative position embeddings and residual pooling connections to integrate the principle of shift-invariance into the model and reduce computational complexity, while the downscaling in MVitv1 is achieved by large strides on the Keys (K) and Values (V).

B. Multi-Classification Tokens (MCT)

MCTs are used to harvest more informative components to achieve good generalizability for AMGE and to construct sender and receiver for cross-modality knowledge distillation in our work. In our MCT setting, we directly use the final layer output of MCT and aggregate the MCT along the token dimension together with Softmax to achieve multi-label classification.

Assuming the classification tokens of MCT to be referred to by $\mathbf{cls}_j, j \in \{1 \dots C\}$ and the flattened patch embeddings to be referred to as $\{\mathbf{p}_i\}, i \in (1, N_{Patches})$ for the given input video, where $N_{Patches}$ is the length of the patch sequence, the input of the first MVitv2 block is $\{\mathbf{cls}_1, \mathbf{cls}_2, \dots, \mathbf{cls}_C, \mathbf{p}_1, \dots, \mathbf{p}_{N_{Patches}}\}$. The final classification is computed through $\mathbf{Output} = \text{Softmax}(\mathbf{P}_\alpha(\sum_{i=1}^C \mathbf{cls}_i/N), \text{dim} = -1)$, where \mathbf{P}_α indicates a fully connected (FC) layer projecting the merged MCT to a single vector with the number of muscle regions as dimensionality. We make use of the same MCT settings for both the video-based backbone and the skeleton-based backbone according to Figure 4. After the first GCN block, the MCT for knowledge distillation and the MCT for classification are added to the model. We first flatten the spatial temporal nodes from the graph structure preserved by the GCN block. We use \mathbf{z}_{GCN} to denote the nodes for the GCN block, \mathbf{cls}_m to denote the MCT for classification, and \mathbf{cls}_r to denote the MCT for knowledge distillation. We then concatenate all of them along the node dimension and do feature projection by using linear projection layer P_m as follows,

$$\mathbf{z}_{GCN}^*, \mathbf{cls}_m^*, \mathbf{cls}_r^* = \text{Split}(\mathbf{P}_m(\text{Cat}(\mathbf{z}_{GCN}^*, \mathbf{cls}_m^*, \mathbf{cls}_r^*))). \quad (1)$$

Then we execute an internal knowledge merge from the nodes to the MCT for the classification, as follows,

$$\hat{\mathbf{cls}}_m = \mathbf{P}_s(\mathbf{z}_{GCN}^*) + \mathbf{cls}_m^*. \quad (2)$$

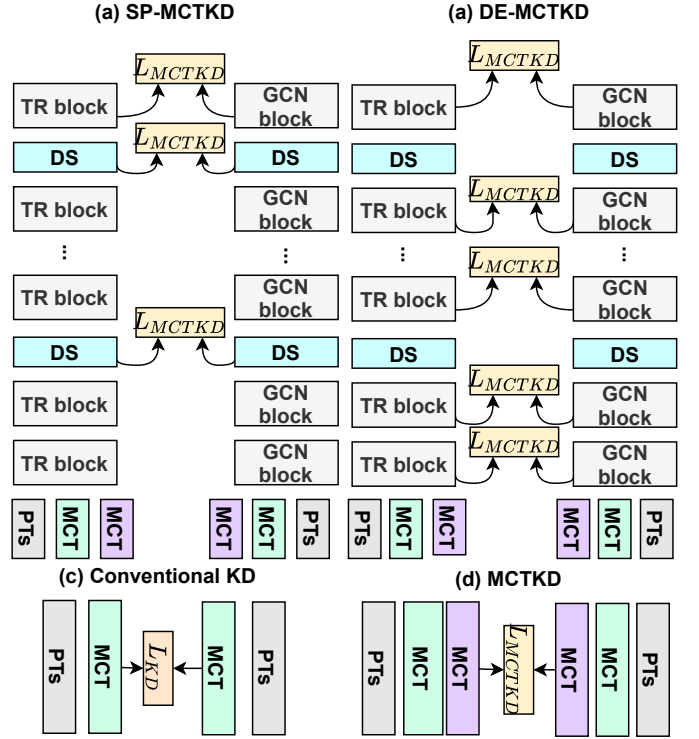


Fig. 5: An overview of the details regarding our ablation study for the MCTKD position and format, where (a) we execute MCTKD after the downsampling of the pooling layer and after the final transformer block to formulate sparse MCTKD, named as SP-MCTKD, (b) we leverage the MCTKD after each transformer block (TR Block) to formulate the dense MCTKD, named as DE-MCTKD, (c) indicates the conventional knowledge distillation (w/o knowledge distillation MCT), and (d) indicates the MCTKD we leveraged.

Finally, the node features, MCT for classification, and MCT for the knowledge distillation will be transferred to the next GCN block and the same procedure will be executed as aforementioned.

C. Multi-Classification Tokens Knowledge Distillation (MCTKD)

Multi-Classification Tokens Knowledge Distillation (MCTKD) is one of our main contributions as shown in Figure 5. To the best of our knowledge, we are the first to introduce this technique which can enable knowledge distillation on the multi-classification tokens between two backbones with obvious structure differences. Through our observation in this work, we find that directly merging the feature from the skeleton-based model and video-based model can not achieve a satisfactory performance due to the huge structure and domain shift between the skeleton domain and the video domain. To achieve appropriate feature fusion between two architectures with obvious differences, we need a new solution focusing on this issue. Knowledge distillation, which has the capability to accomplish the feature space alignment, is firstly explored in our work to assist the cross-modality feature fusion for

the AMGE in-the-wild task. In the past, transformer-based knowledge distillation mainly focused on using intermediate full patch embeddings [37] or final classification token [39], while we propose knowledge distillation on the proposed MCT for both intermediate and final layers by using additional MCT for the knowledge distillation.

The underlying benefit of MCTKD is that the token number of the MCT is fixed, while knowledge distillation on the patch embeddings [38] may encounter the alignment issue when facing different modalities with different token sizes. Instead of directly distilling knowledge from the MCT of an auxiliary modality towards the MCT of a major modality, another N classification token (knowledge distillation MCT) is introduced as aforementioned. This approach avoids disturbing the MCT for classification for the major modality, *i.e.*, RGB video modality. Assuming the knowledge distillation MCT of the major modality branch is denoted as $\text{cls}_r = \{\text{cls}_{r,1}, \text{cls}_{r,2}, \dots, \text{cls}_{r,C}\}$ and the knowledge distillation MCT from the branch of another modality can be indicated by $\text{cls}_s = \{\text{cls}_{s,1}, \text{cls}_{s,2}, \dots, \text{cls}_{s,C}\}$, MCTKD is achieved by applying KL-Divergence (KL-Div) loss after each feature map reduction block of MVITv2 on cls_r and cls_s :

$$L_{MCTKD,all} = \left(\sum_{i=1}^{N_B} KL\text{-Div}(\text{cls}_r^i, \text{cls}_s^i) \right) / N_B, \quad (3)$$

where N_B and $L_{MCTKD,all}$ refer to the block number and the sum of MCTKD losses. $L_{MCTKD,all}$ is combined equally with the binary cross entropy loss (L_{BCE}).

D. Multi-Classification Tokens Fusion (MCTF)

Another major component of TRANSM³E is Multi-Classification Tokens Fusion (MCTF) designed to fuse MCT for knowledge distillation and the original MCT for classification for both of the two models, the process is in Figure 3. Assuming cls_r denotes the knowledge distillation MCT, and cls_m denotes the classification MCT, \mathbf{K} , \mathbf{Q} , and \mathbf{V} for each MCT can be obtained through linear projections:

$$\begin{aligned} \mathbf{K}_m, \mathbf{Q}_m, \mathbf{V}_m &= \mathbf{P}_K^m(\text{cls}_m), \mathbf{P}_Q^m(\text{cls}_m), \mathbf{P}_V^m(\text{cls}_m), \\ \mathbf{K}_r, \mathbf{Q}_r, \mathbf{V}_r &= \mathbf{P}_K^r(\text{cls}_r), \mathbf{P}_Q^r(\text{cls}_r), \mathbf{P}_V^r(\text{cls}_r). \end{aligned} \quad (4)$$

After obtaining the \mathbf{Q} , \mathbf{K} , and \mathbf{V} from the MCT for classification and the MCT for the knowledge, a mixed attention mechanism is calculated as follows,

$$\begin{aligned} \mathbf{A}_{mm}^m &= \mathbf{P}_{mm}(DP(Att(\mathbf{Q}_m, \mathbf{K}_m, \mathbf{V}_m))), \\ \mathbf{A}_{mr}^m &= \mathbf{P}_{mr}(DP(Att(\mathbf{Q}_m, \mathbf{K}_r, \mathbf{V}_m))), \\ \mathbf{A}_{rm}^m &= \mathbf{P}_{rm}(DP(Att(\mathbf{Q}_r, \mathbf{K}_m, \mathbf{V}_m))), \end{aligned} \quad (5)$$

where Att denotes the attention operation computed as $Att(\mathbf{Q}, \mathbf{K}, \mathbf{V}) = \text{Softmax}(\mathbf{Q}@\mathbf{K}) * \mathbf{V}$ and DP indicates Dropout. The above equations provide attention considering different perspectives including self-attention \mathbf{A}_{mm}^m and two types of cross attention, *i.e.* \mathbf{A}_{rm}^m and \mathbf{A}_{mr}^m which use the Queries from the MCT for the classification and the Keys from the MCT for knowledge distillation and vice versa. The same procedure is conducted for the knowledge distillation MCT to generate \mathbf{A}_{rr}^r , \mathbf{A}_{rm}^r , and \mathbf{A}_{mr}^r with Dropout denoted by DP through,

$$\begin{aligned} \mathbf{A}_{rr}^r &= \mathbf{P}_{rr}(DP(Att(\mathbf{Q}_r, \mathbf{K}_r, \mathbf{V}_r))), \\ \mathbf{A}_{rm}^r &= \mathbf{P}_{rm}(DP(Att(\mathbf{Q}_r, \mathbf{K}_m, \mathbf{V}_r))), \\ \mathbf{A}_{mr}^r &= \mathbf{P}_{mr}(DP(Att(\mathbf{Q}_m, \mathbf{K}_r, \mathbf{V}_r))). \end{aligned} \quad (6)$$

Then the attention is finalized as,

$$\begin{aligned} \mathbf{A}_m &= \text{Sum}(\mathbf{A}_{mm}^m, \mathbf{A}_{mr}^m, \mathbf{A}_{rm}^m), \\ \mathbf{A}_r &= \text{Sum}(\mathbf{A}_{rr}^r, \mathbf{A}_{mr}^r, \mathbf{A}_{rm}^r). \end{aligned} \quad (7)$$

The fused attention is thereby calculated through $\mathbf{A}_f = \mathbf{P}_f(\text{Concat}(\mathbf{A}_m, \mathbf{A}_r))$, where \mathbf{P}_f denotes an FC layer. The whole procedure can be indicated by,

$$\mathbf{A}_f = \text{CLS}_f(LN(\text{cls}_m), LN(\text{cls}_r)), \quad (8)$$

where LN demonstrates the layer normalization and CLS_f is the CLS-Fusion. Assuming we use cls_a to denote the average of MCT for classification and the MCT for knowledge distillation by $\text{cls}_a = (\text{cls}_m + \text{cls}_r)/2$, the final fused output is obtained through,

$$\begin{aligned} \text{cls}_f &= \text{cls}_a + \text{CLS}_f(LN(\text{cls}_r), LN(\text{cls}_m)), \\ \text{cls}_f &:= \text{cls}_a + DP(\mathbf{M}_\theta(LN(\text{cls}_f))), \end{aligned} \quad (9)$$

where \mathbf{M}_θ denotes a Multi-Layer Perception (MLP) based projection and DP denoted dropout operation. MCTKD and MCTF are added after N_{MCT} epochs of training of TRANSM³E with only MCT, for both of the leveraged modalities and models. During the test phase, we make use of the average of the prediction results from the two branches as the final prediction.

V. EXPERIMENTS

A. Implementation Details

All the video models are pre-trained on ImageNet1K [79] using PyTorch 1.8.0 with four V100 GPUs. To reproduce TRANSM³E, we first train MVITv2-S with only MCT for classification on RGB modality and HD-GCN with only MCT for classification on skeleton modality for 80 epochs and then train TRANSM³E with all components for another 80 epochs. We use AdamW [87] with learning rate of $1e^{-4}$. The input video for *train*, *test*, and *val* is center cropped and rescaled as 224×224 with color jitter parameter as 0.4.

For our TRANSM³E, we use 16 MVIT-S blocks and choose the number of heads as 1. The feature dimension of the patch embedding net is 96 while using 3D CNN and choosing the patch kernel as $\{3, 7, 7\}$, patch stride kernel as $\{2, 4, 4\}$ and patch padding as $\{1, 3, 3\}$. The MLP ratio for the feature extraction block is 4.0, QKV bias is chosen as True and the path dropout rate is chosen as 0.2. The dimensions of the tokens and number of heads are multiplied by 2 after the 1-st, 3-th, and 14-th blocks. The pooling kernel of QKV is chosen as $\{3, 3, 3\}$, the adaptive pooling stride of KV is chosen as $\{1, 8, 8\}$ while the stride for the pooling on Q is chosen as $\{1, 2, 2\}$ for the 1-st, 3-th, and 14-th block. For the rest of the blocks among 0~15-th blocks, the stride for the pooling on Q is chosen as $\{1, 1, 1\}$. Regarding the MCTF, we choose the head number as 1, the QK scale number as 0.8, the dropout for attention as 0.0, and the dropout rate of

TABLE II: Experimental results on the MuscleMap benchmark. Here, **known val**, **new val**, **known test**, and **new test** denote evaluation and test sets for normal and generalizable validation and test, respectively. **mean val** and **mean test** denote the averaged mean average precision (mAP) of normal and generalizable settings.

Model	#PM	MuscleMap @ mAP					
		known val	new val	mean val	known test	new test	mean test
Random	0.0M	29.7	29.0	29.4	28.9	29.5	29.2
All Ones	0.0M	28.2	28.1	28.2	27.8	28.6	28.2
ST-GCN [21]	2.6M	90.4	63.5	77.0	90.5	63.3	76.9
CTR-GCN [22]	1.4M	93.7	62.2	78.0	93.6	61.7	77.7
HD-GCN [23]	0.8M	93.4	63.1	78.3	93.4	63.1	78.3
C2D (R50) [82]	23.5M	97.2	59.1	78.2	97.4	58.5	78.0
I3D (R50) [19]	20.4M	97.0	59.4	78.2	97.0	58.4	77.7
Slow (R50) [20]	24.3M	96.8	60.7	78.8	96.9	60.5	78.7
SlowFast (R50) [20]	25.3M	89.7	60.2	75.0	94.4	59.6	77.0
MViTv2-S [25]	34.2M	97.7	61.4	79.6	97.9	61.4	79.7
MViTv2-B [25]	51.2M	97.4	61.2	79.3	97.7	61.0	79.4
VideoSwin-S [26]	50.0M	92.6	58.8	75.7	92.4	58.8	75.6
VideoSwin-B [26]	88.0M	91.8	58.7	75.3	91.9	58.3	75.1
TransM³E (Ours)	55.4M	97.8	64.1	81.0	97.8	64.2	81.0

TABLE III: Ablation for TransM³E on the MuscleMap benchmark.

MCT	MCTKD	MCTF	known val	new val	mean val	known test	new test	mean test
✓	✓	✓	95.7	62.1	78.9	95.9	62.0	79.0
✓	✓	✓	95.4	62.4	78.9	95.6	62.1	78.9
✓	✓	✓	97.8	64.1	81.0	97.8	64.2	81.0

TABLE IV: Ablation for KDs for MCTKD on the MuscleMap benchmark.

Method	known val	new val	mean val	known test	new test	mean test
FL-KD	96.5	63.0	79.8	96.4	63.4	79.9
DE-KD	95.9	63.9	79.9	96.6	63.9	80.3
SP-KD	97.5	63.0	80.3	96.7	63.1	79.9
FL-MCTKD	95.1	63.0	79.1	95.5	62.8	79.2
DE-MCTKD	95.1	63.3	79.2	95.2	63.4	79.3
SP-MCTKD	97.8	64.1	81.0	97.8	64.2	81.0

the path as 0.2. The input embeddings of the MCTF have 768 channels while the intermediate embeddings of the MCTF structure have the same number of channels as the input of MCTF. All the hyperparameters are chosen according to the performance measured on the validation set.

B. Analysis on the MuscleMap Benchmark

The results of different architectures on our benchmark are provided in Table II. First, the approaches include *Random*, in which the muscle activation is predicted randomly, and *All Ones*, in which all the samples are predicted as using all the muscle regions. These two simple approaches are used to serve as statistic baselines. *Random* and *All Ones* show overall low performances with <30% mAP on all the evaluations. These statistical approaches are leveraged to make comparisons between deep-learning-based approaches to verify whether the model predicts muscle activation randomly or not. The skeleton-based approach, *e.g.*, HD-GCN [23], ST-GCN [21], and CTR-GCN [22], obviously outperform the

TABLE V: Ablation for the MCTF on the MuscleMap benchmark.

Method	known val	new val	mean val	known test	new test	mean test
Sum [83]	95.4	62.4	78.9	95.6	62.1	78.9
Multiplication [83]	94.5	62.8	78.7	94.7	62.8	78.8
SelfAttention [84]	97.4	62.9	80.2	97.6	62.8	80.2
CrossAttention [84]	94.9	63.7	79.3	95.1	63.5	79.3
MCTF (ours)	97.8	64.1	81.0	97.8	64.2	81.0

TABLE VI: Comparison for MMF/KD on the MuscleMap benchmark.

Method	known val	new val	mean val	known test	new test	mean test
LateFusionSum [83]	80.6	59.8	70.2	80.1	60.0	70.1
LateFusionConcat [85]	83.5	60.8	72.2	83.3	61.2	72.3
LateFusionMul [83]	82.3	60.4	71.4	82.0	60.9	71.5
Ours	97.8	64.1	81.0	97.8	64.2	81.0

statistic approaches and deliver promising performances when dealing with unseen activity types. Video-based approaches surpass statistic and skeleton baselines in terms of the AMGE of the known activities, where transformer-based approaches, *e.g.*, MViTv2 S/B [25] and VideoSwin S/B [26], and CNN-based approaches, *e.g.*, C2D [82], I3D [19], Slow [20], SlowFast [20], are leveraged. MViTv2-S shows good performance compared with the other methods due to the capability for reasoning long-term information and the multi-scale pooling setting which can extract informative cues from different abstract perspectives, especially with 79.6%, 79.7% for **mean val** and **mean test** on the MuscleMap dataset. However, we find that skeleton-based approaches work well on the new activities while they can not deliver satisfactory results on the known activities. On the other hand, video-based approaches work well on the known activities while they can not provide promising AMGE results on the new activities. A good AMGE model is expected to work well in both of the scenarios.

To simultaneously achieve good performances for both the new activities and the known activities, we would like to grasp the advantages both of the skeleton-based approaches

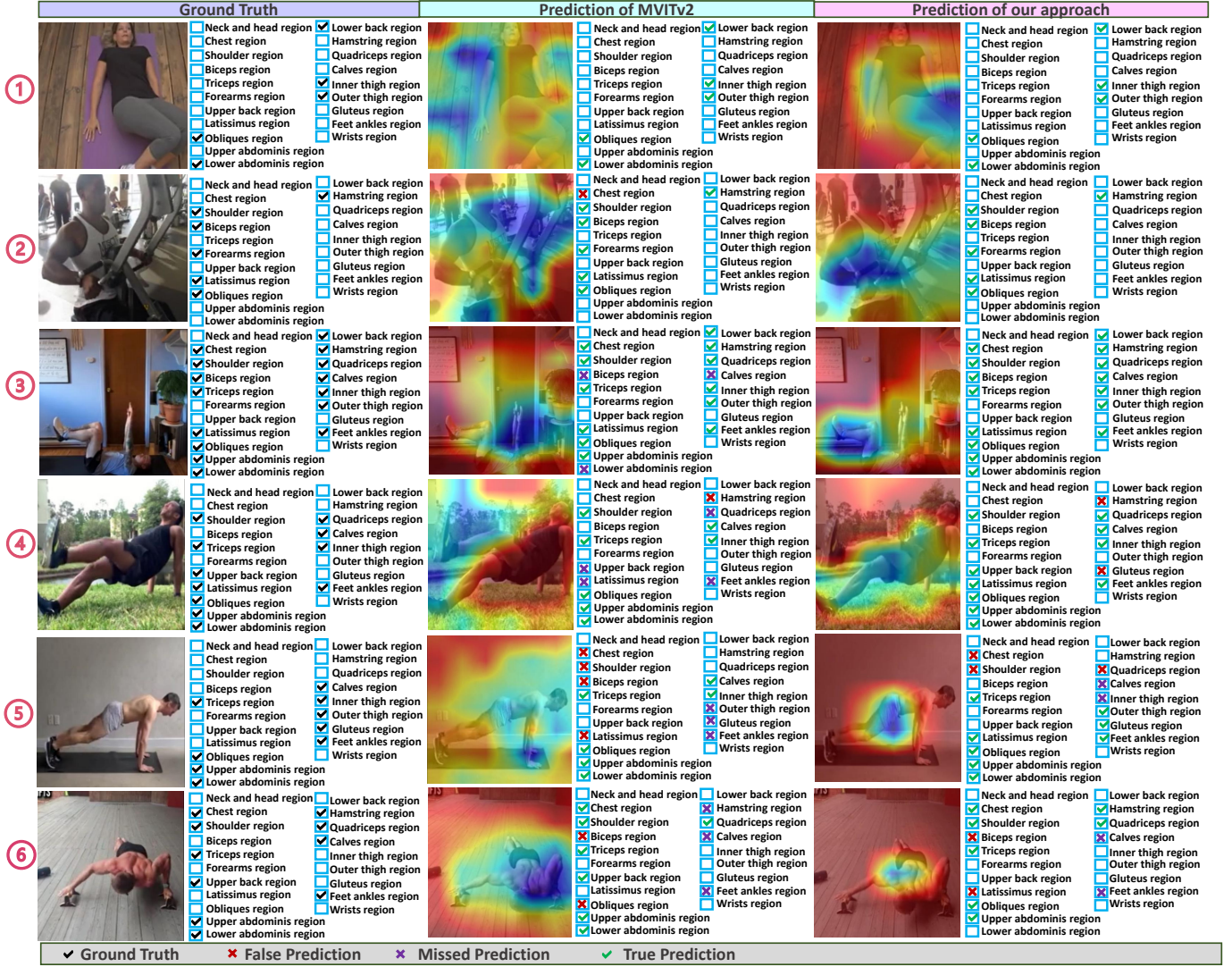


Fig. 6: Qualitative results for the MVitv2-S [25] and TRANSM^{3E}. GradCam [86] visualization is given. The ground truth is shown on the left, and the prediction and gradients of the MVitv2-S [25], and our approach are shown in the middle and on the right.

TABLE VII: Results for different modalities on the Muscle-Map benchmark.

Modality	known val	new val	mean val	known test	new test	mean test
Optical Flow	72.7	59.8	66.3	69.7	57.7	63.7
RGB Difference	96.8	60.3	78.6	97.5	59.8	78.7
RGB	98.5	62.1	80.3	98.6	60.7	79.7

and the video-based approaches. We proposed TRANSM^{3E}, which achieves feature fusion and knowledge distillation by using multi-classification tokens (MCT) on both the video-based model and the skeleton-based model, by using the most outperforming backbones from the two different modalities, *i.e.*, MVitv2-S and HD-GCN. This new proposed method incorporates knowledge distillation from the multi-classification token level and feature fusion from the multi-classification token level to harvest more underlying attributes of the body

motion which can benefit the activated muscle group estimation task in the wild task. TRANSM^{3E} surpasses all the others by large margins. TRANSM^{3E} is a transformer-based approach due to the capability for long-term reasoning of visual transformers [27] since the AMGE should consider the activities at the global level, which requires long-term information reasoning. TRANSM^{3E} has 64.1%, 97.8%, 64.2%, and 81.0% mAP considering **new val**, **known val**, **new test**, and **known test** on our benchmark, while the generalizability to new activities is mostly highlighted. TRANSM^{3E} outperforms MVitv2-S by 1.4% and 1.3% on the **mean val** and **mean test**, which especially works well for **new val** and **new test** as TRANSM^{3E} surpasses MVitv2-S by 2.7% and 2.8%.

The superior performance improvements brought by our proposed method can be attributed to three major factors. First, we make use of MCT to strengthen the attribute reasoning ability during the training phase, which is specifically designed for the multi-class reasoning task. Second, the knowledge

distillation between the video model and the skeleton model achieves a knowledge exchange that could enhance the performance of the proposed model towards both the new and known activities for AMGE. Finally, the fusion between the knowledge distillation MCT and the classification MCT achieves further information aggregation considering the two leveraged modalities. The AMGE performance gap between the known activities and new activities illustrates that our model has the potential to give offensive predictions, misclassification, and biased content which may cause false predictions resulting in a negative social impact. The proposed approach alleviates the generalization problem to a certain degree, however, there is still a large space for further improvement and future research. We will illustrate more analysis of the ablation studies in the following subsection.

C. Analysis of the Ablation Studies

Module ablation. The ablation study of MCT, MCTKD, and MCTF, is shown in Table III, where we deliver the results for *w/o MCT*, *w/o MCTKD*, *w/o MCTF*, and *w/ all*. When we compare the results between *w/o MCT* and *w/ all*, we find that using MCT to enlarge the attributes prediction space can contribute performance improvements by 2.1%, 2.0%, 2.1%, 1.9%, 2.2%, and 2.0% in terms of *known val*, *new val*, *mean val*, *known test*, *new test*, and *mean test*. When comparing the results between *w/o MCTKD* and *w/ all*, we observe that leveraging MCTKD to achieve multi-stage information exchange from the video model and skeleton model can harvest performance improvements by 2.1%, 2.0%, 2.1%, 1.9%, 2.2%, and 2.0% in terms of the six aforementioned evaluations. When we compare the results between *w/o MCTF* and *w/ all*, we find that using MCTF to achieve the fusion between the information derived from the classification MCT and knowledge distillation MCT can bring performance improvements of 2.4%, 1.7%, 2.1%, 2.2%, 2.1%, and 2.1% in terms of the six aforementioned evaluations.

MCTKD ablation. We evaluate the effects of varying the location of knowledge distillation application and the knowledge distillation on a single distillation token (KD) and MCT (MCTKD), where they are named differently, *i.e.*, KD/MCTKD at the final layer (FL-KD/MCTKD), KD/MCTKD after token size reduction (SP-KD/MCTKD), or KD/MCTKD after each MVITv2 block (DE-KD/MCTKD), in Table IV. Considering different knowledge distillation localizations, SP-KD and SP-MCTKD achieve the best performances for KD and MCTKD individually, demonstrating their superiority of using sparse knowledge distillation settings after the reduction of the feature map size. When we compare sparse knowledge distillation with dense knowledge distillation, SP-MCTKD achieves performance improvement by 2.7%, 0.8%, 1.8%, 2.6%, 0.8%, and 1.7% in terms of *known val*, *new val*, *mean val*, *known test*, *new test*, and *mean test*. When we compare sparse knowledge distillation with final layer knowledge distillation, SP-MCTKD achieves performance improvements by 2.7%, 1.1%, 1.9%, 2.3%, 1.4%, and 1.8% in terms of the aforementioned six evaluations. We find that using MCTKD on sparse location setting, *i.e.*, doing MCTKD after each reduction of the feature

map size, delivers the most superior performances on the MuscleMap benchmark, since the AMGE cues from different modalities are highlighted and highly aggregated after the pooling operations, which makes it suitable to achieve an informative knowledge distillation. When we compare the SP-MCTKD with SP-KD, we find that SP-MCTKD outperforms SP-KD. The underlying reason is that through using multi-classification tokens to enlarge the attributes prediction space during the training and feature reasoning, more essential cues for AMGE from different modalities could be better captured and transferred through the knowledge distillation procedure. SP-MCTKD achieves the best performance, thereby it is used to build our proposed model for the knowledge exchange between the skeleton model and the video model.

MCTF ablation. The ablations on MCTF for TRANSM³E are presented in Table V, where our approach is compared with existing fusion approaches, *e.g.*, *Sum*, *Multiplication*, *SelfAttention*, and *CrossAttention*. MCTF shows the best performance with 81.0% and 81.0% on *mean val* and *mean test*. Compared with *CrossAttention*, our MCTF achieves performance improvement by 1.7% and 1.7% in terms of the *mean val* and *mean test*. The superiority of MCTF compared to other attention-based approaches, especially on generalizability, depends on using attention from a more diverse perspective, which benefits the capability of integration considering different focus formats of the attention.

D. Comparison with Conventional Multi-modality Fusion Approaches

Table VI presents the comparison between TRANSM³E and existing multi-modality fusion approaches, *i.e.*, *LateFusionSum*, *LateFusionConcat*, and *LateFusionMul*. We compare our proposed method to these conventional multi-modal fusion approaches to illustrate that the performance improvement of our approach is not solely delivered by using the feature fusion between the skeleton modality and the RGB video modality. Compared with the best performing baseline *LateFusionConcat*, our approach achieves a performance improvement by 14.3%, 3.3%, 8.8%, 4.5%, 3.0%, and 8.7% in terms of *known val*, *new val*, *mean val*, *known test*, *new test*, and *mean test*.

E. Analysis of Different Modalities

We systematically search for the best-performing primary modality considering the video data and present the results in Table VII. We deliver the experimental results on MVITv2-S architecture with MCT pre-trained with ImageNet1K for *Optical Flow*, *RGB Difference*, and *RGB* modalities. We observe that the RGB modality outperforms the other modalities due to its informative temporal-spatial appearance cues which contributes to good AMGE results. We thereby choose the RGB modality as the primary modality to conduct the research and hope that the provided other modalities can enable future research for the multi-modal AMGE.

F. Analysis of Qualitative Results

Qualitative results are shown in Figure 6, the label and GradCam [86] visualizations of MVITv2-S and TRANSM³E

are given from left to right. The true/missed/false prediction is marked as green checkmark/purple crossmark/red crossmark. Overall, our approach has more accurate predictions and less false and missed predictions for all the samples considering known activities, *i.e.*, ①, ② and ③ in Figure 6, and new activities, *e.g.*, ④, ⑤, and ⑥, where ①, ②, and ③ are correctly predicted by our model. TRANSM³E concentrates mostly on the accurate body regions, *e.g.*, in sample ⑤ TRANSM³E focuses on the leg and abdominis related region, while the focus of the MVITv2-S is distracted, which results in more false predictions of MVITv2-S. In sample ④, the arm, abdominal, and leg-related regions of the human body are focused correctly by TRANSM³E.

VI. CONCLUSION

In this paper, we open the vistas of video-based activated muscle group estimation. We contribute the first large-scale video-based activated muscle group estimation dataset considering in-the-wild video and build up MuscleMap benchmark for the AMGE by using statistic baselines and existing video-based approaches including both video-based and skeleton-based methods. We take additional consideration regarding the AMGE generalizability. We propose TRANSM³E with multi-classification token distillation and fusion in a cross-modality manner to enhance the generalization to new activity types. TRANSM³E sets the state-of-the-art on the proposed MuscleMap benchmark. In the future, the utilization of large language models (LLMs) for the purpose of video-based active muscle group estimation is anticipated to enhance the extensibility of the approach with respect to estimating muscle groups during novel physical activities.

REFERENCES

- [1] T. Ahmad, L. Jin, X. Zhang, S. Lai, G. Tang, and L. Lin, "Graph convolutional neural network for human action recognition: A comprehensive survey," *IEEE Transactions on Artificial Intelligence*, vol. 2, no. 2, pp. 128–145, 2021.
- [2] H. Singh, S. Suman, B. N. Subudhi, V. Jakhetiya, and A. Ghosh, "Action recognition in dark videos using spatio-temporal features and bidirectional encoder representations from transformers," *IEEE Transactions on Artificial Intelligence*, vol. 4, no. 6, pp. 1461–1471, 2023.
- [3] T. Zhuang *et al.*, "Temporal refinement graph convolutional network for skeleton-based action recognition," *IEEE Transactions on Artificial Intelligence*, 2023.
- [4] H.-S. Li, J.-Y. Chen, and H.-y. Xia, "Multi-person activity recognition and tracking based on skeletal keypoint detection," *IEEE Transactions on Artificial Intelligence*, 2023.
- [5] A. Jain, R. Akerkar, and A. Srivastava, "Privacy-preserving human activity recognition system for assisted living environments," *IEEE Transactions on Artificial Intelligence*, 2023.
- [6] V. Subbareddy K and N. Devi L, "View invariant spatio-temporal descriptor for action recognition from skeleton sequences," *IEEE Transactions on Artificial Intelligence*, vol. 4, no. 06, pp. 1399–1412, 2023.
- [7] R. D. Estember and C.-J. Huang, "Essential occupational risk and health interventions for Taiwan's bus drivers," in *Proc. ICIEA*, 2019, pp. 273–277.
- [8] T. A. Kuiken, L. A. Miller, R. D. Lipschutz, K. A. Stubblefield, and G. A. Dumanian, "Prosthetic command signals following targeted hyper-reinnervation nerve transfer surgery," in *Proc. EMBAC*, 2006, pp. 7652–7655.
- [9] N. A. Alibeji, V. Molazadeh, F. Moore-Clingenpeel, and N. Sharma, "A muscle synergy-inspired control design to coordinate functional electrical stimulation and a powered exoskeleton: Artificial generation of synergies to reduce input dimensionality," *IEEE Control Systems Magazine*, vol. 38, no. 6, pp. 35–60, 2018.
- [10] F. I. Rahma, R. Mawan, H. Harianto, and Kusrimi, "Nutrition and lifestyle recommendations for patients recovering from covid-19 in nusa tenggara barat province," in *Proc. ICORIS*, 2020, pp. 1–6.
- [11] A. W. de Vries, F. Krause, and M. P. de Looze, "The effectivity of a passive arm support exoskeleton in reducing muscle activation and perceived exertion during plastering activities," *Ergonomics*, vol. 64, no. 6, pp. 712–721, 2021.
- [12] T. Liang and Y. J. Yuan, "Wearable medical monitoring systems based on wireless networks: A review," *IEEE Sensors Journal*, vol. 16, no. 23, pp. 8186–8199, 2016.
- [13] Y. Bababekova, M. Rosenfield, J. E. Hue, and R. R. Huang, "Font size and viewing distance of handheld smart phones," *Optometry and Vision Science*, vol. 88, no. 7, pp. 795–797, 2011.
- [14] S. Seneviratne *et al.*, "A survey of wearable devices and challenges," *IEEE Communications Surveys & Tutorials*, vol. 19, no. 4, pp. 2573–2620, 2017.
- [15] F. R. Williams, A. Berzigotti, J. M. Lord, J. C. Lai, and M. J. Armstrong, "Impact of exercise on physical frailty in patients with chronic liver disease," *Alimentary Pharmacology & Therapeutics*, 2019.
- [16] D. Sanchez-Lorente, R. Navarro-Ripoll, R. Guzman, J. Moises, E. Gimeno, M. Boada, and L. Molins, "Prehabilitation in thoracic surgery," *Journal of Thoracic Disease*, 2018.
- [17] Y. Lu, Y. Wang, and Q. Lu, "Effects of exercise on muscle fitness in dialysis patients: A systematic review and meta-analysis," *American Journal of Nephrology*, vol. 50, no. 4, pp. 291–302, 2019.
- [18] M. Chiquier and C. Vondrick, "Muscles in action," in *Proc. ICCV*, 2023, pp. 22091–22101.
- [19] J. Carreira and A. Zisserman, "Quo vadis, action recognition? A new model and the kinetics dataset," in *Proc. CVPR*, 2017, pp. 4724–4733.
- [20] C. Feichtenhofer, H. Fan, J. Malik, and K. He, "SlowFast networks for video recognition," in *Proc. ICCV*, 2019, pp. 6201–6210.
- [21] S. Yan, Y. Xiong, and D. Lin, "Spatial temporal graph convolutional networks for skeleton-based action recognition," in *Proc. AAAI*, 2018, pp. 7444–7452.
- [22] Y. Chen, Z. Zhang, C. Yuan, B. Li, Y. Deng, and W. Hu, "Channel-wise topology refinement graph convolution for skeleton-based action recognition," in *Proc. ICCV*, 2021, pp. 13339–13348.
- [23] J. Lee, M. Lee, D. Lee, and S. Lee, "Hierarchically decomposed graph convolutional networks for skeleton-based action recognition," *arXiv preprint arXiv:2208.10741*, 2022.
- [24] H. Fan *et al.*, "Multiscale vision transformers," in *Proc. ICCV*, 2021, pp. 6804–6815.
- [25] Y. Li *et al.*, "MVITv2: Improved multiscale vision transformers for classification and detection," in *Proc. CVPR*, 2022, pp. 4794–4804.
- [26] Z. Liu *et al.*, "Video swin transformer," in *Proc. CVPR*, 2022, pp. 3192–3201.
- [27] A. Vaswani *et al.*, "Attention is all you need," in *Proc. NeurIPS*, 2017, pp. 5998–6008.
- [28] S. Kang and R. P. Wildes, "Review of action recognition and detection methods," *arXiv preprint arXiv:1610.06906*, 2016.
- [29] K. Soomro, A. R. Zamir, and M. Shah, "UCF101: A dataset of 101 human actions classes from videos in the wild," *arXiv preprint arXiv:1212.0402*, 2012.
- [30] H. Kuehne, H. Jhuang, E. Garrote, T. Poggio, and T. Serre, "HMDB: A large video database for human motion recognition," in *Proc. ICCV*, 2011, pp. 2556–2563.
- [31] F. Caba Heilbron, V. Escorcia, B. Ghanem, and J. Carlos Niebles, "ActivityNet: A large-scale video benchmark for human activity understanding," in *Proc. CVPR*, 2015, pp. 961–970.
- [32] K. Peng, A. Roitberg, K. Yang, J. Zhang, and R. Stiefelhofen, "Should I take a walk? Estimating energy expenditure from video data," in *Proc. CVPRW*, 2022, pp. 2074–2084.
- [33] P. Parmar and B. T. Morris, "What and how well you performed? A multitask learning approach to action quality assessment," in *Proc. CVPR*, 2019, pp. 304–313.
- [34] J. Xu, Y. Rao, X. Yu, G. Chen, J. Zhou, and J. Lu, "FineDiving: A fine-grained dataset for procedure-aware action quality assessment," in *Proc. CVPR*, 2022, pp. 2939–2948.
- [35] D. Shao, Y. Zhao, B. Dai, and D. Lin, "FineGym: A hierarchical video dataset for fine-grained action understanding," in *Proc. CVPR*, 2020, pp. 2613–2622.
- [36] G. E. Hinton, O. Vinyals, and J. Dean, "Distilling the knowledge in a neural network," *arXiv preprint arXiv:1503.02531*, 2015.
- [37] A. Monti, A. Porrello, S. Calderara, P. Coscia, L. Ballan, and R. Cucchiara, "How many observations are enough? Knowledge distillation for trajectory forecasting," in *Proc. CVPR*, 2022, pp. 6543–6552.

- [38] Z. Fang, J. Wang, X. Hu, L. Wang, Y. Yang, and Z. Liu, "Compressing visual-linguistic model via knowledge distillation," in *Proc. ICCV*, 2021, pp. 1408–1418.
- [39] H. Touvron, M. Cord, M. Douze, F. Massa, A. Sablayrolles, and H. Jégou, "Training data-efficient image transformers & distillation through attention," in *Proc. ICML*, 2021, pp. 10 347–10 357.
- [40] R. Liu *et al.*, "TransKD: Transformer knowledge distillation for efficient semantic segmentation," *arXiv preprint arXiv:2202.13393*, 2022.
- [41] M. C. Tosin, J. C. Machado, and A. Balbinot, "sEMG-based upper limb movement classifier: Current scenario and upcoming challenges," *Journal of Artificial Intelligence Research*, vol. 75, pp. 83–127, 2022.
- [42] K. R. Berckmans, B. Castelein, D. Borms, T. Parlevliet, and A. Cools, "Rehabilitation exercises for dysfunction of the scapula: exploration of muscle activity using fine-wire EMG," *The American Journal of Sports Medicine*, vol. 49, no. 10, pp. 2729–2736, 2021.
- [43] C. Feichtenhofer, A. Pinz, and A. Zisserman, "Convolutional two-stream network fusion for video action recognition," in *Proc. CVPR*, 2016, pp. 1933–1941.
- [44] J. Donahue *et al.*, "Long-term recurrent convolutional networks for visual recognition and description," in *Proc. CVPR*, 2015, pp. 2625–2634.
- [45] K. Peng, A. Roitberg, K. Yang, J. Zhang, and R. Stiefelwagen, "TransDARC: Transformer-based driver activity recognition with latent space feature calibration," in *Proc. IROS*, 2022, pp. 278–285.
- [46] Z. Liu *et al.*, "Swin transformer V2: Scaling up capacity and resolution," in *Proc. CVPR*, 2022, pp. 11 999–12 009.
- [47] Y. Tang *et al.*, "Uncertainty-aware score distribution learning for action quality assessment," in *Proc. CVPR*, 2020, pp. 9836–9845.
- [48] A. J. Piergiovanni, A. Angelova, and M. S. Ryoo, "Evolving losses for unsupervised video representation learning," in *Proc. CVPR*, 2020, pp. 130–139.
- [49] M. Patrick, Y. M. Asano, R. Fong, J. F. Henriques, G. Zweig, and A. Vedaldi, "Multi-modal self-supervision from generalized data transformations," *arXiv preprint arXiv:2003.04298*, 2020.
- [50] J.-B. Alayrac *et al.*, "Self-supervised multimodal versatile networks," in *Proc. NeurIPS*, 2020, pp. 25–37.
- [51] D. Schneider, S. Sarfraz, A. Roitberg, and R. Stiefelwagen, "Pose-based contrastive learning for domain agnostic activity representations," in *Proc. CVPRW*, 2022, pp. 3432–3442.
- [52] R. Panda *et al.*, "AdaMML: Adaptive multi-modal learning for efficient video recognition," in *Proc. ICCV*, 2021, pp. 7556–7565.
- [53] L. Shi, Y. Zhang, J. Cheng, and H. Lu, "Two-stream adaptive graph convolutional networks for skeleton-based action recognition," in *Proc. CVPR*, 2019, pp. 12 026–12 035.
- [54] —, "Skeleton-based action recognition with multi-stream adaptive graph convolutional networks," *IEEE Transactions on Image Processing*, vol. 29, pp. 9532–9545, 2020.
- [55] V. Choutas, P. Weinzaepfel, J. Revaud, and C. Schmid, "PoTion: Pose motion representation for action recognition," in *Proc. CVPR*, 2018, pp. 7024–7033.
- [56] H. Duan, Y. Zhao, K. Chen, D. Lin, and B. Dai, "Revisiting skeleton-based action recognition," in *Proc. CVPR*, 2022, pp. 2959–2968.
- [57] J. Gou, B. Yu, S. J. Maybank, and D. Tao, "Knowledge distillation: A survey," *International Journal of Computer Vision*, vol. 129, no. 6, pp. 1789–1819, 2021.
- [58] X. Jin *et al.*, "Knowledge distillation via route constrained optimization," in *Proc. ICCV*, 2019, pp. 1345–1354.
- [59] B. Zhao, Q. Cui, R. Song, Y. Qiu, and J. Liang, "Decoupled knowledge distillation," in *Proc. CVPR*, 2022, pp. 11 943–11 952.
- [60] Z. Zhang, C. Zhou, and Z. Tu, "Distilling inter-class distance for semantic segmentation," in *Proc. IJCAI*, 2022, pp. 1686–1692.
- [61] Z. Yang, Z. Li, M. Shao, D. Shi, Z. Yuan, and C. Yuan, "Masked generative distillation," in *Proc. ECCV*, 2022, pp. 53–69.
- [62] P. Chen, S. Liu, H. Zhao, and J. Jia, "Distilling knowledge via knowledge review," in *CVPR*, 2021.
- [63] Y. Lee, K. Jang, J. Goo, Y. Jung, and H. Kim, "FitHuBERT: Going thinner and deeper for knowledge distillation of speech self-supervised learning," *arXiv preprint arXiv:2207.00555*, 2022.
- [64] C. Pham, L. Nguyen, A. Nguyen, N. Nguyen, and V.-T. Nguyen, "Combining skeleton and accelerometer data for human fine-grained activity recognition and abnormal behaviour detection with deep temporal convolutional networks," *Multimedia Tools and Applications*, vol. 80, no. 19, pp. 28 919–28 940, 2021.
- [65] E. Kazakos, A. Nagrani, A. Zisserman, and D. Damen, "EPIC-Fusion: Audio-visual temporal binding for egocentric action recognition," in *Proc. ICCV*, 2019, pp. 5491–5500.
- [66] T. Ridnik *et al.*, "Asymmetric loss for multi-label classification," in *Proc. ICCV*, 2021, pp. 82–91.
- [67] R. You, Z. Guo, L. Cui, X. Long, Y. Bao, and S. Wen, "Cross-modality attention with semantic graph embedding for multi-label classification," in *Proc. AAAI*, 2020, pp. 12 709–12 716.
- [68] J. Ye, J. He, X. Peng, W. Wu, and Y. Qiao, "Attention-driven dynamic graph convolutional network for multi-label image recognition," in *Proc. ECCV*, 2020, pp. 649–665.
- [69] Z.-M. Chen, X.-S. Wei, P. Wang, and Y. Guo, "Multi-label image recognition with graph convolutional networks," in *Proc. CVPR*, 2019, pp. 5177–5186.
- [70] V. Sovrasov, "Combining metric learning and attention heads for accurate and efficient multilabel image classification," *arXiv preprint arXiv:2209.06585*, 2022.
- [71] S. Liu, L. Zhang, X. Yang, H. Su, and J. Zhu, "Query2Label: A simple transformer way to multi-label classification," *arXiv preprint arXiv:2107.10834*, 2021.
- [72] S. Xu, Y. Li, J. Hsiao, C. Ho, and Z. Qi, "A dual modality approach for (zero-shot) multi-label classification," *arXiv preprint arXiv:2208.09562*, 2022.
- [73] Q. Gao, J. Liu, and Z. Ju, "Hand gesture recognition using multimodal data fusion and multiscale parallel convolutional neural network for human-robot interaction," *Expert Systems*, 2021.
- [74] K. Peng, A. Roitberg, K. Yang, J. Zhang, and R. Stiefelwagen, "Delving deep into one-shot skeleton-based action recognition with diverse occlusions," *IEEE Transactions on Multimedia*, vol. 25, pp. 1489–1504, 2023.
- [75] H. Zhao, Z. Yan, L. Torresani, and A. Torralba, "HACS: Human action clips and segments dataset for recognition and temporal localization," in *Proc. ICCV*, 2019, pp. 8667–8677.
- [76] A. Li, M. Thotakuri, D. A. Ross, J. Carreira, A. Vostrikov, and A. Zisserman, "The AVA-Kinetics localized human actions video dataset," *arXiv preprint arXiv:2005.00214*, 2020.
- [77] R. F. Escamilla *et al.*, "Core muscle activation during Swiss ball and traditional abdominal exercises," *Journal of Orthopaedic & Sports Physical Therapy*, vol. 40, no. 5, pp. 265–276, 2010.
- [78] D. H. Hardwick, J. A. Beebe, M. K. McDonnell, and C. E. Lang, "A comparison of serratus anterior muscle activation during a wall slide exercise and other traditional exercises," *Journal of Orthopaedic & Sports Physical Therapy*, vol. 36, no. 12, pp. 903–910, 2006.
- [79] J. Deng, W. Dong, R. Socher, L. Li, K. Li, and L. Fei-Fei, "ImageNet: A large-scale hierarchical image database," in *Proc. CVPR*, 2009, pp. 248–255.
- [80] L. Buitinck *et al.*, "API design for machine learning software: experiences from the scikit-learn project," in *Proc. ECMLW*, 2013.
- [81] A. Dosovitskiy *et al.*, "An image is worth 16x16 words: Transformers for image recognition at scale," in *Proc. ICLR*, 2021.
- [82] C. Feichtenhofer, A. Pinz, and R. P. Wildes, "Spatiotemporal multiplier networks for video action recognition," in *Proc. CVPR*, 2017, pp. 7445–7454.
- [83] A. Roitberg, K. Peng, Z. Marinov, C. Seibold, D. Schneider, and R. Stiefelwagen, "A comparative analysis of decision-level fusion for multimodal driver behaviour understanding," in *Proc. IV*, 2022, pp. 1438–1444.
- [84] A. Nagrani, S. Yang, A. Arnab, A. Jansen, C. Schmid, and C. Sun, "Attention bottlenecks for multimodal fusion," in *Proc. NeurIPS*, 2021, pp. 14 200–14 213.
- [85] P.-C. Wei, K. Peng, A. Roitberg, K. Yang, J. Zhang, and R. Stiefelwagen, "Multi-modal depression estimation based on sub-attentional fusion," in *Proc. ECCV*, 2022, pp. 623–639.
- [86] R. R. Selvaraju, M. Cogswell, A. Das, R. Vedantam, D. Parikh, and D. Batra, "Grad-CAM: Visual explanations from deep networks via gradient-based localization," in *Proc. ICCV*, 2017, pp. 618–626.
- [87] I. Loshchilov and F. Hutter, "Decoupled weight decay regularization," in *Proc. ICLR*, 2019.